



Nano-iron oxide-catalyzed selective oxidations of alcohols and olefins with hydrogen peroxide

Feng Shi^a, Man Kin Tse^{a,b}, Marga-Matina Pohl^c, Jörg Radnik^c,
Angelika Brückner^c, Shengmao Zhang^d, Matthias Beller^{a,b,*}

^a Leibniz-Institut für Katalyse e.V. an der Universität Rostock, Albert-Einstein-Str. 29a, 18059 Rostock, Germany

^b Center for Life Science Automation (CELISCA), University of Rostock, Friedrich-Barnewitz-Str. 8, D-18119 Rostock-Warnemünde, Germany

^c Leibniz-Institut für Katalyse e.V. an der Universität Rostock, Außenstelle Berlin, Richard-Willstätter-Str. 3, 12489 Berlin, Germany

^d Special Functional Material Laboratory, Henan University, 475001 Kaifeng, China

ARTICLE INFO

Article history:

Received 3 April 2008

Received in revised form 6 June 2008

Accepted 19 June 2008

Available online 27 June 2008

Keywords:

Nano-catalysts

Iron oxide

Oxidation

Green chemistry

Hydrogen peroxide

Alcohols

ABSTRACT

Unsupported “free” nano- γ -Fe₂O₃ is an active, stable, and reusable catalyst for selective oxidations of alcohols and olefins applying hydrogen peroxide as terminal oxidant. Catalyst activity and selectivity are controlled by tuning the particle size. The formation of a thin carbon-layer on the surface of the nano-iron oxide during the reaction permits for high catalyst stability. All catalysts were characterized by TEM, X-ray photoelectron spectroscopy (XPS), XRD, and EPR.

© 2008 Elsevier B.V. All rights reserved.

1. Introduction

Selective oxidation reactions constitute industrial core technologies for converting bulk chemicals to useful products of a higher oxidation state [1,2]. Nevertheless, they represent problematic transformations and still most of the known textbook oxidation reactions are unacceptable with regard to selectivity and waste generation. Clearly, traditional methods using stoichiometric quantities of inorganic oxidants such as chromium(VI) reagents, permanganates, or *N*-chlorosuccinimide (NCS) are not environmentally benign [3]. Even more recent developments of hypervalent iodine reagents, which are popular in organic synthesis, also cause severe environmental problems. Hence, the development of greener oxidation systems applying less poisonous catalysts, oxidants, and solvents became an important goal for catalysis [4]. Beside pure oxygen/air, hydrogen peroxide is one of the ideal candidates of green oxidants for selective oxidation reactions [5]. Theoretically, the only by-product produced is water. Thus, high

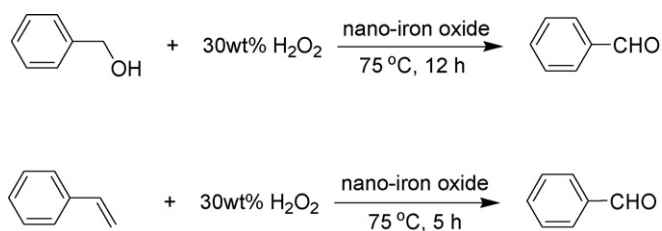
atom efficiency (47%) can be realized. In the past mainly transition metal complexes based on vanadium, molybdenum, titanium, tungsten, ruthenium, osmium, platinum and iron have been studied as catalysts for selective oxidation reactions with hydrogen peroxide as the oxidant [6–15].

Although iron plays wonderfully as oxidation catalyst in nature, the difficulty to stabilize this metal as catalyst centre and prevent non-selective reactions makes its usage as catalyst on laboratory scale, but especially for industrial production, more troublesome. Nonetheless, since the end of last century, iron catalysis has become a “hot topic” due to the obvious advantages such as availability and price. Traditionally, iron is normally used as Lewis acid in homogeneous catalysis or as catalyst or support in heterogeneous catalysis [16–20]. With respect to oxidation catalysis notable progress has been accomplished in recent years and novel iron containing systems have been developed for hydroxylation [21–23], sulfide oxidation [24,18,25], epoxidation [26–30], and alcohol oxidation [31,32]. Among almost all iron complexes, iron oxides have been often considered to be catalytically inactive under mild reaction conditions. However, some iron oxides can be used as magnetically separable support [33–36].

In a preliminary communication, we have shown that nano-iron oxide is an active and selective catalyst for alcohol and olefin oxidation to yield the corresponding aldehydes (Scheme 1) [37]. Here, we

* Corresponding author at: Leibniz-Institut für Katalyse e.V. an der Universität Rostock, Albert-Einstein-Str. 29a, D-18059 Rostock, Germany.
Tel.: +49 381 1281 113; fax: +49 381 1281 5000.

E-mail address: matthias.beller@katalyse.de (M. Beller).



Scheme 1. Selective oxidation of benzyl alcohol and styrene to benzaldehyde using hydrogen peroxide as oxidant.

report the detailed characterization of the nano-iron oxide catalysts and their activity for selective oxidations is discussed.

2. Experimental

2.1. Materials

Bulk α -Fe₂O₃ (product No.: 31005-0, >100 nm) and nano- γ -Fe₂O₃ **1** (product No.: 544884, 20–50 nm) were purchased from Aldrich. Nano- γ -Fe₂O₃ **2** and bulk γ -Fe₂O₃ were prepared according to reported methods [38,39]. All commercial chemicals were directly used without any purification. The catalysts used in this work are shown in Table 1.

2.2. Characterization

For particle size analysis, a transmission electron microscope CM20 STWIN (Philips) equipped with an energy dispersive X-ray spectrometer (EDXS) PV9900 (EDAX) was used at 200 kV. For TEM investigations the catalysts were dispersed by an ultrasonic bath in ethanol and deposited on carbon-coated copper grids. The PV9900 allowed qualitative and quantitative measurements of elements above Na.

XRD measurements were conducted by a STADI P automated transmission diffractometer (STOE) equipped with an incident beam curved germanium monochromator selecting Cu K α 1 radiation and a 6° position sensitive detector (PSD). The XRD patterns were scanned in the 2 θ range of 5–60° (step width: 0.5°, 100 s per step). For the data interpretation the software WinXpov (STOE) and the database of powder diffraction file (PDF) of the International Centre of Diffraction Data (ICDD) were used.

The X-ray photoelectron spectroscopy (XPS) measurements were carried out on a VG ESCALAB220iXL spectrometer with Al K α radiation ($E = 1486.6$ eV). The samples were fixed by a double-sided adhesive carbon tape on a stainless steel sample holder. The electron binding energy was referenced to the O 1s peak of Fe₂O₃ at 529.6 eV. The peaks were fitted by Gaussian–Lorentzian curves after a Shirley background subtraction. For quantitative analysis, the peak area was divided by the element-specific Scofield factor and the transmission function of the analyser. The background pressure in the chamber was better than 10^{−7} Pa.

Table 1
Iron oxide catalysts and corresponding particle size estimated by TEM

Entry	Catalysts	Particle size (nm)
1	Bulk α -Fe ₂ O ₃	>100
2	Bulk γ -Fe ₂ O ₃	>100
3	Nano- γ -Fe ₂ O ₃ 1	20–50 ^a
4	Nano- γ -Fe ₂ O ₃ 2	3–5
5	Fe(NO ₃) ₃ ·9H ₂ O/FeCl ₃ ·6H ₂ O	–
6	Nano- γ -Fe ₂ O ₃ 1 used 1 time	20–50 ^a
7	Nano- γ -Fe ₂ O ₃ 1 used 5 times	20–50 ^a

^a Size of the majority of the particles.

EPR spectra were recorded at 77 K and at room temperature by an ELEXSYS 500-10/12 cw-spectrometer (Bruker) with a microwave power of 0.63 mW, a receiver gain of 25 db, a modulation amplitude of 1 G and a modulation frequency of 100 kHz.

2.3. Reaction conditions for selective oxidations

General procedure for selective oxidations of benzyl alcohol: All reactions were carried out with a multi-reactor (Carousel 12 station, RADLEYS). To a glass reactor (~50 mL), benzyl alcohol (1081 mg, 10.0 mmol) and 1 mol% of nano-Fe₂O₃ **1** (16.0 mg) were added, respectively. The reaction mixture was vigorously stirred (500–750 rpm) at 75 °C. H₂O₂ (30 wt% in water, from VWR, 1.0 mL, 10.0 mmol) were added continuously in 12 h. The mixture was then cooled to room temperature and 1,4-dioxane (1760 mg, 20 mmol) was added as an internal standard for quantitative analysis by GC-FID. The conversion was 33%, selectivity was 97% and the GC yield was 32%. Three-time reproducibility testing showed the yield was in the range of 29–33%.

General procedure for selective oxidations of cyclooctanol: All reactions were carried out with a multi-reactor (Carousel 12 station, RADLEYS). To a glass reactor (~50 mL), cyclooctanol (1282 mg, 10.0 mmol) and 1 mol% of nano-Fe₂O₃ **1** (16.0 mg) were added, respectively. The reaction mixture was vigorously stirred (500–750 rpm) at 75 °C. H₂O₂ (30 wt% in water, from VWR, 1.5 mL, 15.0 mmol) were added continuously in 12 h. The mixture was then cooled to room temperature and 1,4-dioxane (1760 mg, 20 mmol) was added as an internal standard for quantitative analysis by GC-FID.

General procedure for selective oxidations of olefins: All reactions were carried out in an oil bath (75 °C, oil bath temperature). To a glass reactor (~50 mL), olefin (10.0 mmol), H₂O₂ (30 wt% in water, from VWR, 2.0 ml, 20.0 mmol) and 1 mol% of nano-Fe₂O₃ **1** (16.0 mg) were added, respectively. The reaction was vigorously stirred (500–750 rpm) at 75 °C for 5 h. The mixture was then cooled to room temperature and 1,4-dioxane (1760 mg, 20 mmol) was added as internal standard for quantitative analysis by GC-FID. The conversion was 19%, selectivity was >99% and the GC yield was 19%.

Scale-up experiment for selective oxidation of benzyl alcohol: The reaction was carried out in an oil bath (75 °C, oil bath temperature). To a round bottom flask (250 mL), benzyl alcohol (31.6 g, 200 mmol) and 1 mol% of nano-Fe₂O₃ **1** (320 mg) were added, respectively. The reaction mixture was vigorously stirred (500–750 rpm) at 75 °C. H₂O₂ (30 wt% in water, from VWR, 20 ml, 200 mmol) were added continuously in 12 h. The mixture was then cooled to room temperature and 1,4-dioxane (35.2 g, 400 mmol) was added as internal standard for quantitative analysis by GC-FID. The reaction was repeated twice, the average conversion was 26%, selectivity was 96% and the GC yield was 25%.

Qualitative and quantitative analysis were carried out with a GC-FID (HP6890N with FID detector, column HP5 30 m × 0.250 mm × 0.25 μ m) and GC-MS (HP6890N with MSD5973, column HP5MS 30 m × 0.250 mm × 0.25 μ m) and compared with the authentic samples.

3. Results and discussion

3.1. Results of TEM characterization

The bulk α -Fe₂O₃ contains particles with an anisotropic shape in the range of some 100 nm, Fig. 1. The sample is stable within the electron beam and shows lattice planes (0.36 nm, 0.3 nm) which are typical for different iron oxide structures. Thus, from TEM no determination of the particular crystal structure can be made. However, as shown below this is possible by XRD. In some cases amorphous

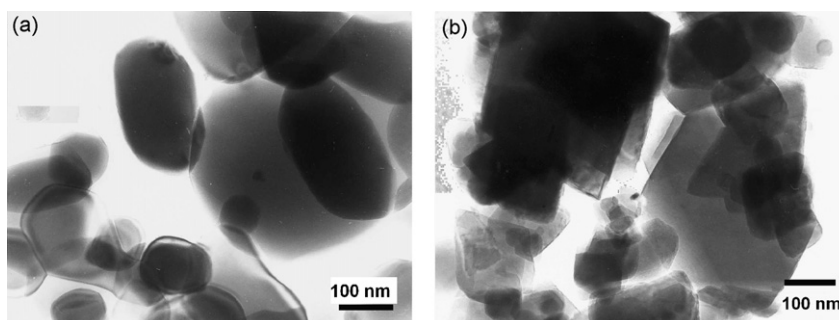


Fig. 1. TEM pictures of (a) bulk- α - Fe_2O_3 and (b) bulk- γ - Fe_2O_3 .

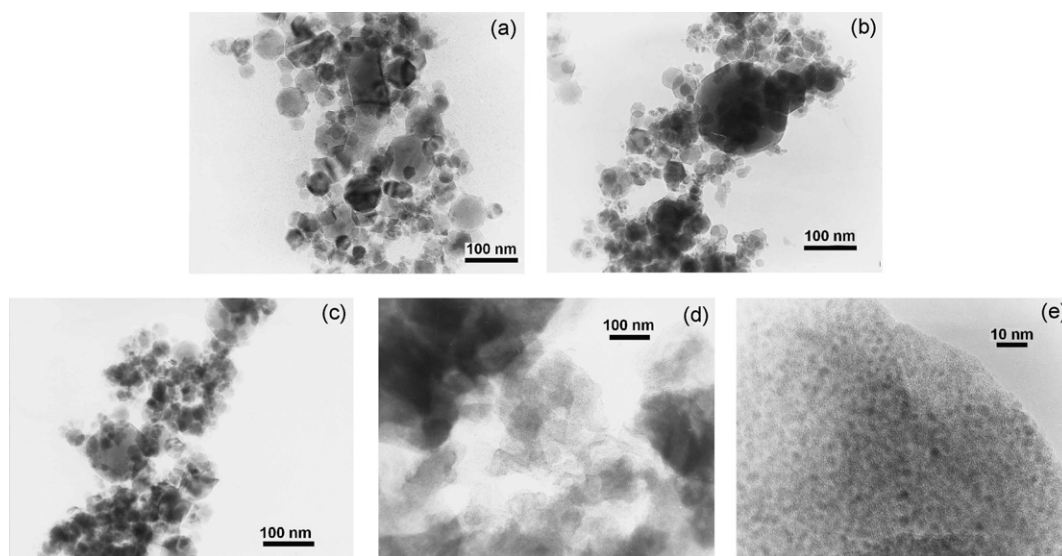


Fig. 2. TEM pictures of nano- γ - Fe_2O_3 **1** (a), nano- γ - Fe_2O_3 **1** reused 1 time (b), nano- γ - Fe_2O_3 **1** reused 5 times (c) and nano- γ - Fe_2O_3 **2** (d and e).

skins of about 2 nm with weak contrast are observed at the surface of particles. Similar particle size, >100 nm, as for the bulk α - Fe_2O_3 was observed in bulk γ - Fe_2O_3 sample and the lattice planes respond to γ - Fe_2O_3 exhibited in Fig. 2.

For nano- γ - Fe_2O_3 **1**, Fig. 2a, and nano- γ - Fe_2O_3 **1** (reused 1 and 5 times) Fig. 2b and c particle sizes from 10 to more than 200 nm were found, the majority of the particles being between 20 and 50 nm. The largest particles were observed within the fresh sample and have a diameter of about 350 nm. In the used samples the largest particles were slightly smaller, presenting diameters between 200 and 300 nm. However, the overall shape and size distribution in the samples after reuse does not differ from the fresh nano- γ - Fe_2O_3 **1**, which particle sizes are mainly in the range of 20–50 nm. Furthermore, the fresh sample of nano- γ - Fe_2O_3 was sensitive against the electron beam. Thus, lattice planes could only be observed during the first 10 s of beam exposure, which is too short to take micrographs. All other used samples were more stable. At the same time, after 5 times of reuse in cyclooctanol oxidation, an amorphous layer appeared on the maghemite crystallites, which was not seen after single use. According to XPS results discussed below, this layer most probably consists of carbon.

As shown in Fig. 2d the sample of nano- γ - Fe_2O_3 **2** consists of large particles with an anisotropic shape. At higher magnification the fine structure of the sample was visible (Fig. 2e). Within an amorphous matrix, dark dots of about 3–5 nm were observed which originate from iron oxide. In some cases, these dots showed weak lattice planes of 0.31 nm.

3.2. Results of XRD analysis

Based on XRD analysis the crystal structure of the different samples is confirmed (Fig. 3). The XRD patterns of bulk α - Fe_2O_3 are characteristic of hematite. The reflections of bulk γ - Fe_2O_3 , nano- γ - Fe_2O_3 **1**, and nano- γ - Fe_2O_3 **1** reused 1 and 5 times could be due to both magnetite or maghemite. For a statistical distribution of the cationic defects in the lattice, maghemite has the same

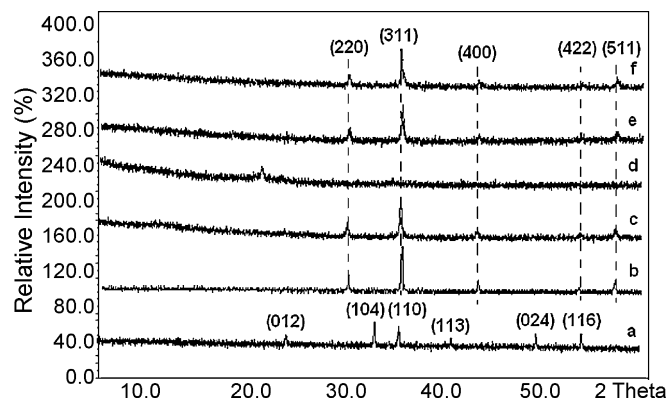


Fig. 3. XRD direction patterns of different iron oxide catalysts. (a) Bulk α - Fe_2O_3 , (b) bulk γ - Fe_2O_3 , (c) nano- γ - Fe_2O_3 **1**, (d) nano- γ - Fe_2O_3 **2**, (e) nano- γ - Fe_2O_3 **1** used 1 time, and (f) nano- γ - Fe_2O_3 **1** used 5 times.

crystal structure as magnetite and discrimination exclusively from XRD is difficult. However, the XPS results presented below suggest that iron atoms are almost exclusively trivalent in these samples. Therefore, the XRD reflections were assigned to maghemite, which contains only trivalent Fe^{3+} . As can be seen from Fig. 3, there are virtually no differences in the powder patterns of nano- $\gamma\text{-Fe}_2\text{O}_3$ **1** before and after reuse, suggesting that the iron oxide catalyst did not change during its use in alcohol oxidation. This is in good agreement with the TEM results discussed above.

The interpretation of the results obtained from nano- $\gamma\text{-Fe}_2\text{O}_3$ **2** is more difficult, since only one weak peak is found in the XRD pattern. This agrees with the TEM results which suggest a very small particle size of 3–5 nm. This may be at the detection limit of XRD.

3.3. Results of XPS analysis

Fig. 4 depicts the Fe 2p spectra of the different samples. All Fe 2p spectra show the typical structure for iron oxides with broad main peaks ($\text{Fe } 2p_{3/2}$ and $\text{Fe } 2p_{1/2}$) and typical shake-up satellites. Electron binding energies of the $\text{Fe } 2p_{3/2}$ peaks between 710.0 and 710.5 eV are observed for the sample of bulk $\alpha\text{-Fe}_2\text{O}_3$, which corresponds to trivalent Fe.

The XPS spectra of bulk and nano- $\gamma\text{-Fe}_2\text{O}_3$ **1** are rather similar to the spectra of bulk $\alpha\text{-Fe}_2\text{O}_3$. The position of the main peaks is characteristic of trivalent Fe. In contrast to bulk $\alpha\text{-Fe}_2\text{O}_3$, a small so-called “pre-peak” can be observed in nano- $\gamma\text{-Fe}_2\text{O}_3$ **1** before and

after reuse. This peak may arise from Fe ions with a lower oxidation state than **3** in the neighbourhood of defect sites. Thus, it cannot be completely excluded that trace amounts of iron with lower valence states (such as Fe^{2+}) may be present in the sample. However, their amount is certainly much smaller than it would be required for an Fe_3O_4 phase.

Interestingly, the Fe signal intensity decreased after recycling the catalyst for 5 times, while a single use in the oxidation of cyclooctanol had no remarkable influence on the Fe 2p peak intensity (Fig. 4). Simultaneously to the decrease of the Fe 2p intensity, a significant increase of the C 1s intensity (not shown) was observed. To quantify this effect, the C/Fe ratio for the near-surface region was calculated from the C 1s and Fe 2p peaks. It increased from 0.64 in the fresh sample to 2.82 after 5 times use. This result indicates that the Fe ions are covered by carbon containing compounds during the reaction.

This agrees well with the results of TEM analyses which revealed the presence of an amorphous over-layer on the nano- $\gamma\text{-Fe}_2\text{O}_3$ **1** after 5 times of reuse, but not on nano- $\gamma\text{-Fe}_2\text{O}_3$ **1**, which was reused for 1 time. Considering the binding energy (BE) values of the $\text{Fe } 2p_{3/2}$ electrons of nano- $\gamma\text{-Fe}_2\text{O}_3$ **1** (5 times reuse), a shift of about 1 eV to lower BE values is observed. This is typical for a strong interaction between carbon and the Fe ions. For nano- $\gamma\text{-Fe}_2\text{O}_3$ **2**, much more carbon was observed in the near-surface region (C/Fe = 54.3). Here, relative weak Fe 2p peaks were detected with a binding energy of 709.3 eV, which points to the interaction of Fe^{3+} with carbon (Fig. 4). A similar binding energy was also observed for the recycled (5 times) nano- $\gamma\text{-Fe}_2\text{O}_3$ **1**.

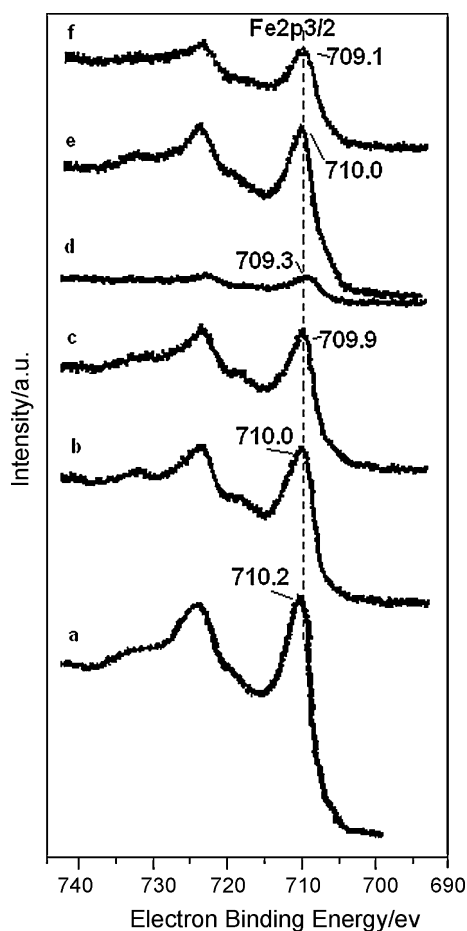


Fig. 4. XPS spectra (Fe 2p signals) of different iron oxide catalysts. (a) Bulk $\alpha\text{-Fe}_2\text{O}_3$, (b) bulk $\gamma\text{-Fe}_2\text{O}_3$, (c) nano- $\gamma\text{-Fe}_2\text{O}_3$ **1**, (d) nano- $\gamma\text{-Fe}_2\text{O}_3$ **2**, (e) nano- $\gamma\text{-Fe}_2\text{O}_3$ **1** used 1 time, and (f) nano- $\gamma\text{-Fe}_2\text{O}_3$ **1** used 5 times.

3.4. Results of EPR analysis

Due to the EPR-silence of $\alpha\text{-Fe}_2\text{O}_3$, here, the EPR measurements were mainly used to test the stability of nano- $\gamma\text{-Fe}_2\text{O}_3$ **1** during reaction. EPR spectra of nano- $\gamma\text{-Fe}_2\text{O}_3$ **1** before and after reuse show very intense asymmetric signals (Fig. 5). Such line shapes are characteristic for ferri- and ferromagnetic resonance (FMR) in magnetic materials such as maghemite and magnetite. Thus, the signals might arise from ferromagnetic resonance within maghemite particles (as detected by TEM and XRD in agreement with XPS). The signal anisotropy is due to the anisotropic orientation of the spin domains within the magnetic particles which are frozen at low temperature. As thermal fluctuations gain importance with increasing temperature, this anisotropy is averaged out, which will lead to narrower and isotropic signals [40]. This is not yet the case for the rather large particles in samples deriving from nano- $\gamma\text{-Fe}_2\text{O}_3$ **1**. The intensity of an FMR signal, which is proportional to the magnetization, does not depend on temperature well below the Curie point. Near the Curie point, a steep intensity decrease occurs and the sample becomes paramagnetic. For maghemite, the Curie temperature is not known since it is above the conversion to hematite ($\alpha\text{-Fe}_2\text{O}_3$) which occurs at 673 K. In any case, the spectra in Fig. 5 have been recorded well below the Curie temperature. Accordingly, the intensity measured at 77 K and at room temperature is almost the same. No significant change of the line shape and intensity were observed after being reused in the reactions. This agrees well with results of TEM and XRD, which do not point to significant structural changes during the catalytic reactions. Moreover, it is consistent with TEM results, which revealed the presence of rather large particles with sizes above 10 nm.

For the sample of nano- $\gamma\text{-Fe}_2\text{O}_3$ **2** the signal intensity and the anisotropy are markedly reduced in comparison to nano- $\gamma\text{-Fe}_2\text{O}_3$ **1**. This is characteristic for superparamagnetic particles [41]. In contrast to ferri- or ferromagnetic particles, superparamagnetic particles have negligible remnant magnetization but a very large magnetic moment. Such behaviour is usually observed for very

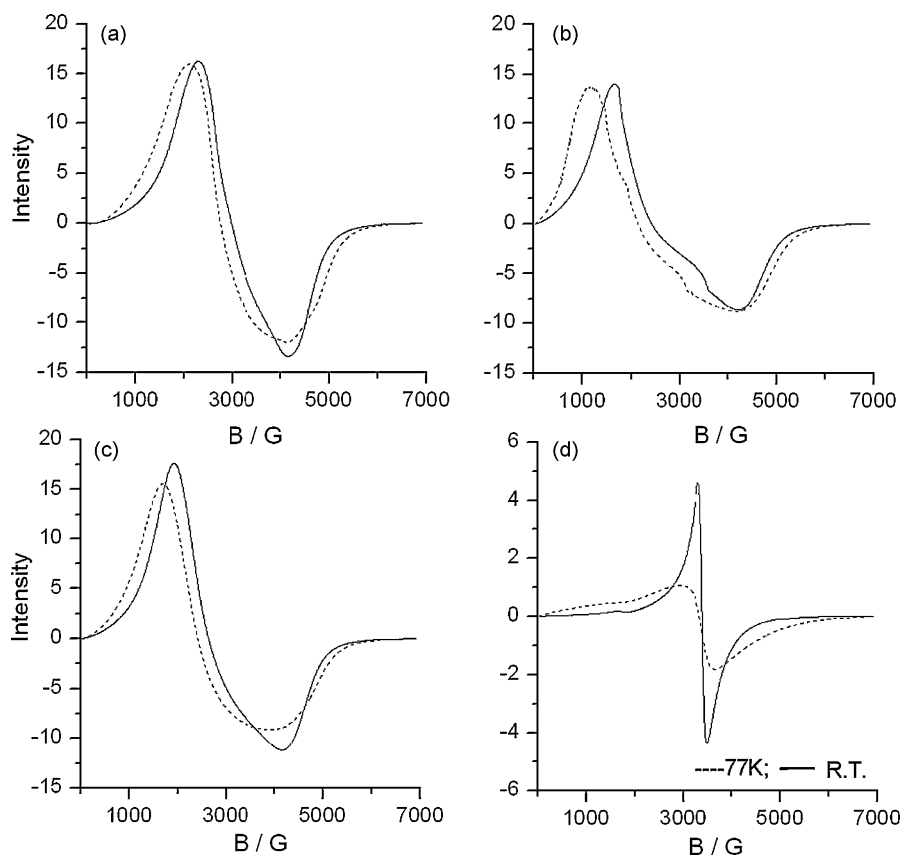


Fig. 5. EPR spectra of nano- γ -Fe₂O₃ **1** (a), nano- γ -Fe₂O₃ **1** used 1 time (b), 5 times (c) and nano- γ -Fe₂O₃ **2** (d).

small particles with diameters in the 1–10 nm range. The spectra plotted in Fig. 5d suggests that sample nano- γ -Fe₂O₃ **2** might contain a magnetically ordered phase similar to nano- γ -Fe₂O₃ **1**, however, with a remarkable smaller particle size. This is in line with TEM results (showing particles of 3–5 nm in size) and also with XRD.

3.5. Oxidation of benzyl alcohol to benzaldehyde

The oxidation of benzyl alcohol to benzaldehyde was used as model reaction. Initially, optimization of the reaction conditions and influence of the different catalysts were investigated

[37]. The results for the catalyst screening are shown in Table 2. As expected bulk α -Fe₂O₃ and γ -Fe₂O₃ (particle size >100 nm, Fig. 1 a and b) are poorly active. Here, conversions of around 5% and low catalyst turnover numbers (TONs) are obtained (Table 2, entries 1 and 2). Higher catalyst activity is achieved when nano- γ -Fe₂O₃ with a particle size in the range of 20–50 nm was applied (Fig. 2a). In this case the conversion reached 33% together with 97% selectivity (Table 2, entry 3). When nano- γ -Fe₂O₃ with smaller particle size is employed (3–5 nm, Fig. 2d and e), higher activity is obtained (86% conversion), but the chemoselectivity decreased severely at the same time (35%) (Table 2, entry 4). Notably, this result is similar to the homogeneous iron catalyst system.

Table 2
Selective oxidation of benzyl alcohol to benzaldehyde^a

Entry	Catalyst (%)	H ₂ O ₂ (equiv.)	Conversion (%)	Selectivity (%)	TON ^b
1	Bulk α -Fe ₂ O ₃ (1)	1	~5	99	5
2	Bulk γ -Fe ₂ O ₃ (1)	1	~5	99	4
3	Nano- γ -Fe ₂ O ₃ 1 (1)	1	33	97	32
4	Nano- γ -Fe ₂ O ₃ 2 (1)	1	86	35	30
5	FeCl ₃ ·6H ₂ O (1)	1	90	21	19
6	Fe(NO ₃) ₃ ·9H ₂ O (1)	1	71	35	25
7	Nano- γ -Fe ₂ O ₃ 1 (0.2)	1	6	99	30
8	Nano- γ -Fe ₂ O ₃ 1 (0.5)	1	18	97	35
9	Nano- γ -Fe ₂ O ₃ 1 (2)	1	41	88	18
10	Nano- γ -Fe ₂ O ₃ 1 (4)	1	47	85	10
11	Nano- γ -Fe ₂ O ₃ 1	1.5	72	66	12
12 ^c	Nano- γ -Fe ₂ O ₃ 1	1	26	96	25

^a 10 mmol of benzyl alcohol (1.08 g), 1.0 equiv. of H₂O₂ (10 mmol, 1.0 mL, 30 wt% in water), 1 mol% of catalyst, 75 °C, 12 h. The H₂O₂ was added continuously in 12 h.

^b Mol of aldehyde produced per mol of catalyst.

^c 200 mmol of benzyl alcohol, 200 mmol of H₂O₂ (30 wt% in water), 1 mol% of catalyst, 75 °C, 12 h. The reactions were performed 2 times and the results were the average number.

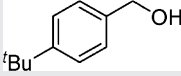
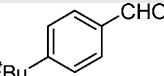
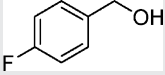
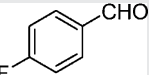
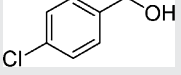
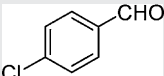
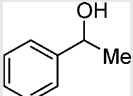
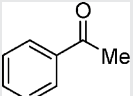
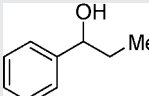
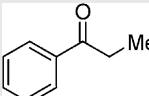
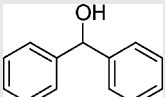
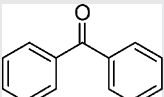
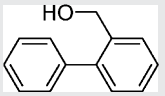
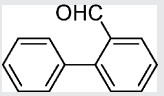

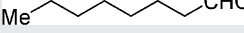
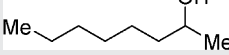
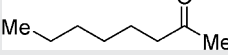
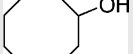
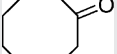
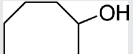
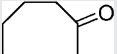
Here, 70–90% conversion and 20–35% selectivity are obtained in the presence of $\text{Fe}(\text{NO}_3)_3 \cdot 9\text{H}_2\text{O}$ or $\text{FeCl}_3 \cdot 6\text{H}_2\text{O}$ (Table 2, entries 5 and 6).

Apparently, with decreasing particle size of nano-iron oxide its catalytic properties were changed to become similar to the homogeneous iron salt system. Hence, it is possible by controlling the particle size to tune the catalytic activity between the bulk and the homogenous catalyst system! Advantageously, the ferromagnetic property of $\gamma\text{-Fe}_2\text{O}_3$ makes the isolation and recycling of the catalyst easy. On laboratory scale in the presence of a magnetic stirrer bar, the $\gamma\text{-Fe}_2\text{O}_3$ was absorbed on to its surface when the stirring was stopped. Next, the catalyst loadings were further optimized from 0.2% to 4%. It is clear, with increasing catalyst amount, the conversion increased simultaneously but the selectivity and TONs decreased (Table 2, entries 7–10). For example, the conversion reached 47% with 4 mol% of $\gamma\text{-Fe}_2\text{O}_3$ but the selectivity decreased to 85%. Adding more hydrogen peroxide, i.e. 1.5 equiv., the chemose-

lectivity decreased to 66% (Table 2, entry 11). It is worth mentioning that the nano-iron oxide catalyst system is relatively easy to be scaled up (Table 2, entry 12).

The main reason for the improved activity of nano-iron oxide probably originates from the nanolization of the bulk-iron oxide. In general, nanolization of heterogeneous catalysts offer higher surface areas, which lead to more low-coordination sites and surface vacancies. These are responsible for the higher catalyst activity [42–44]. Theoretically it can be assumed that, with a decrease of the particle size down to a “molecular” level, the nano-catalyst behave as a homogeneous system, in which the catalytic activity is not controlled by the surface area of the catalyst but governed by the concentration [45]. The most important significance of these results is that “free” nano- Fe_2O_3 but not immobilized nano- Fe_2O_3 is highly active, selective and stable by merely controlling the particle size. Although there is no direct evidence, the partial exclusion of the radical mechanism maybe one of the

Table 3
Selective oxidation of alcohols to aldehydes and ketones with nano- $\gamma\text{-Fe}_2\text{O}_3$ ^{1a}

Entry	Substrate	Product	Conversion (%)	Selectivity (%)	TON
1			10	>99	10
2			87	51	44
3			98	61	60
4			42	60	25
5			35	42	44
6			49	52	25
7			6	>99	6
8			–	–	–
9			6	>99	6
10			14	>99	14
11 ^b			15	>99	70 ^c

^a Reaction conditions similar to Table 1, except that 1.5 equiv. of hydrogen peroxide is used.

^b The catalyst was used 5 times.

^c Total turnover number of 5 experiments.

possible reasons for the high selectivity of the nano-iron oxide catalysts.

3.6. Selective oxidation of different alcohols

Then, the scope of nano-iron oxide for selective oxidation of different alcohols was tested. As shown in Table 3 substitutions on the aromatic ring of the benzyl alcohol have considerable impact on the catalyst activity. For *tert*-butyl-substituted benzyl alcohol, excellent selectivity (99%) towards the corresponding aldehyde was obtained, although the conversion was relatively low (Table 3, entry 1). For halogen-substituted benzyl alcohols, the nano- γ -Fe₂O₃ exhibited higher activity but the selectivity decreased to 50–60% (Table 3, entries 2–3). Other alcohols such as 1-phenylethanol, diphenylmethanol and 1-phenyl-1-propanol, gave good conversions, but the selectivity was lower in comparison with benzyl alcohol (Table 3, entries 4–6). On the other hand very high selectivity was observed when 2-biphenylmethanol was applied (Table 3, entry 7).

Aliphatic alcohols are more difficult to be oxidized. In fact, there only 6% conversion was observed for 2-octanol (Table 3, entry 9). However, 15% conversion with 99% selectivity was achieved for

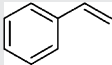
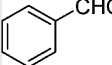
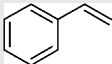
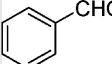
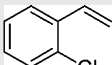
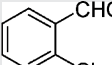
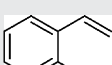
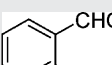
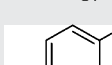
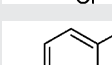
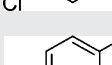
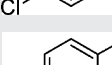
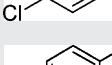
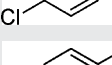
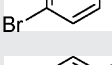
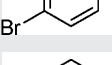
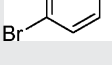
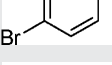
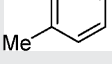
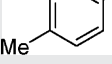
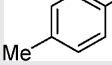
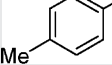
cyclooctanol (Table 3, entry 10). We further used this reaction to test the reusability of the nano-iron oxide. For this purpose the catalyst was attracted onto the surface of the magnetic stirrer bar after the reaction. Then, it was washed with acetone, dried in air, and directly reused for the next reaction without any further treatment. No significant loss of catalyst activity is observed even after 5 times reuse (Table 3, entry 11).

3.7. Selective oxidation of olefins

As shown in our preliminary communication nano- γ -Fe₂O₃ **1** does not only catalyze the oxidation of alcohols to carbonyl compounds [37]. Moreover, aromatic olefins can be smoothly oxidatively cleaved to the corresponding aldehydes in the presence of **1** (Table 4). In order to get information about the efficiency of the catalyst, two catalyst loadings (0.5% and 1%) were tested.

It is apparent that lower conversions but higher TONs were achieved with 0.5% nano- γ -Fe₂O₃ **1**. In contrast to the alcohol oxidations, styrene and its halogen-substituted derivatives exhibited high activity and chemoselectivity (>99%). Among all the olefins tested in this work, the highest catalyst activity is exhibited by

Table 4
Selective oxidation of olefins to aldehydes with nano- γ -Fe₂O₃ **1**^a

Entry	Substrates	Product	Catalyst (mol%)	Conversion (%)	Selectivity (%)	TON ^b
1			1	19	100	19
2			0.5	13	100	26
3			1	31	100	31
4			0.5	17	100	34
5			1	17	100	17
6			0.5	13	100	26
7			1	14	~00	14
8			0.5	10	~100	20
9			1	48	75	36
10			0.5	28	71	40
11			1	–	–	–

^a 10 mmol olefin, 1 mol% catalyst, alcohol:H₂O₂ = 1:2 (1 equiv. mol/mol), 75 °C, 5 h. The H₂O₂ was added at the beginning.

^b Mol aldehyde produced per mol catalyst.

4-methyl styrene (conversion: 48%, TON=36) with 75% selectivity. Unfortunately, aliphatic 1-octene is not oxidized at all (Table 4, entry 11).

4. Conclusions

In conclusion, nano- γ -Fe₂O₃ is shown to be an active, stable and selective catalyst for the oxidation of alcohols and styrenes with hydrogen peroxide as terminal oxidant. High selectivity with acceptable activity was achieved by tuning the particle size of nano-iron oxide into the range of 20–50 nm. With this catalyst benzyl alcohols and styrene derivatives are easily oxidized into corresponding carbonyl compounds with good to excellent selectivity. For aliphatic alcohols and olefins, only the cyclic and secondary alcohols are oxidized. The results presented here should be helpful to understand the relationship between homogeneous and heterogeneous catalysis.

Acknowledgments

This work has been supported by the State of Mecklenburg-Western Pomerania, the Deutsche Forschungsgemeinschaft (SPP 1118 and Leibniz prize) and the Bundesministerium für Bildung und Forschung (BMBF). Dr. Feng Shi thanks the Alexander-von-Humboldt-Stiftung for an AvH-Fellowship.

References

- [1] J.E. Bäckvall (Ed.), *Modern Oxidation Methods*, Wiley–VCH, 2004.
- [2] S.M. Roberts, *Catalysts for Fine Chemical Synthesis*, Wiley–VCH, 2007.
- [3] R.A. Sheldon, J.K. Kochi, *Metal-catalyzed Oxidation of Organic Compounds*, Academic, New York, 1981.
- [4] R.A. Sheldon, I.W.C.E. Arends, U. Isabel, *Green Chemistry and Catalysis*, Wiley–VCH, 2007.
- [5] C. W. Jones, *Application of Hydrogen Peroxide and Derivatives*; Royal Society of Chemistry: Cambridge, 1999.
- [6] R. Curci, J.O. Edwards, G. Strukul, *Catalytic Oxidations with Hydrogen Peroxide as Oxidant*, Kluwer, Dordrecht, 1992, pp. 46–96, Chapter 3.
- [7] T. Matsumoto, M. Ueno, N. Wang, S. Kobayashi, *Chem. Asian J.* 3 (2008) 196.
- [8] F. Shi, M. Tse, M. Beller, *Chem. Asian J.* 2 (2007) 415.
- [9] F. Shi, M.K. Tse, M. Beller, *J. Mol. Catal.* 270 (2007) 68.
- [10] M.K. Tse, S. Bhor, M. Klawonn, C. Döbler, M. Beller, *Tetrahedron Lett.* 44 (2003) 479.
- [11] M.K. Tse, S. Bhor, M. Klawonn, G. Anilkumar, H. Jiao, C. Döbler, A. Spannenberg, W. Mägerlein, H. Hugl, M. Beller, *Chem. Eur. J.* 12 (2006) 1855.
- [12] C. Döbler, G. Mehlretter, M. Beller, *Angew. Chem. Int. Ed.* 38 (1999) 3026.
- [13] B.S. Lane, K. Burgess, *Chem. Rev.* 103 (2003) 2457.
- [14] G. Grigoropoulou, J.H. Clark, J.A. Elings, *Green Chem.* 5 (2003) 1.
- [15] I.W.C.E. Arends, R.A. Sheldon, *Top. Catal.* 19 (2002) 133.
- [16] C. Bolm, J. Legros, J. Le Paih, L. Zani, *Chem. Rev.* 104 (2004) 6217.
- [17] M. Costas, K. Chen, L. Que Jr., *Coord. Chem. Rev.* 200–202 (2000) 517.
- [18] J. Legros, C. Bolm, *Angew. Chem. Int. Ed.* 43 (2004) 4225.
- [19] B. Moens, H. De Winne, S. Corthals, H. Poelman, R. De Gryse, V. Meynen, P. Cool, B.F. Sels, P.A. Jacobs, *J. Catal.* 247 (2007) 86.
- [20] T. Riedel, H. Schulz, G. Schaub, J. Jun, K. Lee, *Top. Catal.* 26 (2003) 41.
- [21] For a recent minireview on iron catalysts for oxidations and hydrogenations see: S. Enthaler, K. Junge, M. Beller, *Angew. Chem. Int. Ed.* 47, 2008, 2323–2333.
- [22] M. Fujita, M. Costas, L. Que Jr., *J. Am. Chem. Soc.* 125 (2003) 9912.
- [23] P.D. Oldenburg, A.A. Shteinman, L. Que Jr., *J. Am. Chem. Soc.* 127 (2005) 15672.
- [24] J. Legros, C. Bolm, *Chem. Eur. J.* 11 (2005) 1086.
- [25] J. Legros, C. Bolm, *Angew. Chem. Int. Ed.* 42 (2003) 5487.
- [26] F.G. Gelalcha, B. Bitterlich, G. Anilkumar, M.-K. Tse, M. Beller, *Angew. Chem. Int. Ed.* 46 (2007) 7293.
- [27] K. Schröder, X. Tong, B. Bitterlich, M.K. Tse, F.G. Gelalcha, A. Brückner, M. Beller, *Tetrahedron Lett.* 48 (2007) 6339.
- [28] G. Anilkumar, B. Bitterlich, F. Gadissa Gelalcha, M.K. Tse, M. Beller, *Chem. Commun.* (2007) 289.
- [29] N.A. Stephenson, A.T. Bell, *J. Am. Chem. Soc.* 127 (2005) 8635.
- [30] G. Dubois, A. Murphy, T.D.P. Stack, *Org. Lett.* 5 (2003) 2469.
- [31] M. Nakanishi, C. Bolm, *Adv. Syn. Catal.* 349 (2007) 861.
- [32] S.E. Martín, A. Garrone, *Tetrahedron Lett.* 44 (2003) 549.
- [33] A.-H. Lu, E.L. S Salabas, F. Schüth, *Angew. Chem. Int. Ed.* 46 (2007) 1222.
- [34] R. Abu-Reziq, H. Alper, D. Wang, M.L. Post, *J. Am. Chem. Soc.* 128 (2006) 5279.
- [35] C. Dálaigh, S.A. Corr, Y. Gun'ko, S.J. Connon, *Angew. Chem. Int. Ed.* 46 (2007) 4329.
- [36] A. Hu, G.T. Yee, W. Lin, *J. Am. Chem. Soc.* 127 (2005) 12486.
- [37] F. Shi, M.K. Tse, M.M. Pohl, A. Brückner, S. Zhang, M. Beller, *Angew. Chem. Int. Ed.* 46 (2007) 8866.
- [38] A.B. Bourlino, A. Simopoulos, D. Petridis, *Chem. Mater.* 14 (2002) 899.
- [39] M. Ozaki, E. Matijević, *J. Colloid Interface Sci.* 107 (1985) 199.
- [40] C. Cannas, D. Gatteschi, A. Musinu, G. Piccaluga, C. Sangregorio, *J. Phys. Chem. B* 102 (1998) 7721.
- [41] L. Bonneviot, M. Che, D. Olivier, G.A. Martin, E. Freund, *J. Phys. Chem.* 90 (1986) 2112.
- [42] G. Pacchioni, *Surf. Rev. Lett.* 7 (2000) 277.
- [43] W.D. Knight, K. Clemenger, W.A. de Heer, W.A.M. Saunders, Y. Chou, M.L. Cohen, *Phys. Rev. Lett.* 52 (1984) 2141.
- [44] A. Kaldor, D. Cox, M.R. Zakin, *Adv. Chem. Phys.* 70 (1988) 211.
- [45] Y. Zhao, K. Aoki, *Chem. Phys. Lett.* 430 (2006) 117.